Journal of Molecular Structure 985 (2011) 173–183

Contents lists available at ScienceDirect

Journal of Molecular Structure

journal homepage: www.elsevier.com/locate/molstruc

DNA interaction, Enhanced DNA photocleavage, electrochemistry, thermal investigation and biopotencial properties of new mixed-ligand complexes of Cu(II)/VO(IV) based on Schiff bases

Natarajan Raman *, Abraham Selvan

Research Department of Chemistry, VHNSN College, Virudhunagar 626 001, India

ARTICLE INFO

Article history:
Received 9 September 2010
Received in revised form 20 October 2010
Accepted 21 October 2010
Available online 3 November 2010

Keywords:
Metal complex
Polypyridyl ligand
DNA interaction
DNA photocleavage
Antimicrobial activity

ABSTRACT

Using the Schiff base ligand, **dbdppo** (4-(3′,4′-dimethoxybenzaldehydene)2-3-dimethyl-1-phenyl-3-pyrazolin-5-one or **hnbdppo** (4-(3′-hydroxy-4′-nitrobenzaldehydene)2-3-dimethyl-1-phenyl-3-pyrazolin-5-one with polypyridyl ligand(s) as co-ligand(s), Cu(II) and VO(IV) complexes have been synthesized and characterized by the physicochemical properties. The electrochemical properties, DNA binding affinities, as well as photonuclease activities of the complexes, were examined in detail. The DNA binding characteristics of the Cu(II) and VO(IV) complexes was investigated by spectroscopic, electrochemical and viscosity measurements. The UV–Vis, and magnetic moment data revealed an octahedral geometry around Cu(II) ion and square-pyramidal geometry around VO(IV) ion and conductivity data conveyed the electrolytic nature of the complexes. The spectroscopic studies together with cyclic voltammetry and viscosity experiments support that both of the complexes bound to CT DNA by partial intercalation into the base pairs of DNA. Moreover, these complexes have been found to promote the photocleavage of plasmid DNA pBR322 under irradiation at 365 nm. Further, the synthesized ligands, in comparison to their metal complexes were screened for their antimicrobial activity against bacterial and fungal species. The activity data show that the metal complexes have more antimicrobial potent than the parent Schiff base ligands.

1. Introduction

Antipyrine and its derivatives have been widely used as pharmaceuticals due to broad bioactivities as antitumor [1], antimicrobial [2,3], antiviral [4], and analgesic [5], *etc*. Nowadays, antipyrine derivatives (APDs) have been accepted as important biomodel compounds in the biological and medical fields [6]. In recent years, APDs have exhibited attractive multi-functional properties as coordinate [7], antioxidant [8] antiputrefactive [9] and optical [10] characteristics in chemical and material fields.

Schiff bases are characterized by the —N=CH— (imine) group which is important in elucidating the mechanism of transamination and rasemination reaction in biological system [11]. Moreover, the incorporation of transition metal into Schiff bases enhances the biological activity of the ligand and decreases the cytotoxic effects of both the metal ion and ligand on the host [12].

Studies on the interaction of transition metal complexes with DNA continue to attract the attention of researchers due to their importance in design and development of synthetic restriction enzymes, chemotherapeutic drugs and DNA foot printing agents [13,14]. DNA is an important cellular receptor, many chemicals exert their antitumor effects by binding to DNA thereby changing the replication of DNA and inhibiting the growth of the tumor cells, which is the basis of designing new and more efficient antitumor drugs and their effectiveness depends on the mode and affinity of the binding [15].

Despite a considerable amount of literature on metal complex–DNA interaction, the knowledge of the nature of binding of the complexes to DNA and their binding geometries has remained a subject of intense debate. On the other hand, as compared with the intercalative ligand, the influence of the ancillary ligands of the complexes has received little attention. Since the octahedral polypyridyl Cu(II) complexes bind to DNA in three dimensions, the ancillary ligands can also play an important role in governing DNA-binding of these complexes. At the same time, varying substitutive group or substituent position in the ligands can also create some interesting differences in the space configuration and the electron density distribution of Cu(II) and VO(IV) polypyridyl complexes, which will seed some differences in spectral properties and the DNA-binding behaviors of the complexes, and will also helpful in clearly understanding the binding mechanism of Cu(II) and VO(IV) polypyridyl complexes to DNA.

In this communication, we describe the chelation behavior of Schiff base derived from the condensation of 4-aminoantipyrine with 3,4-disubstituted aromatic aldehydes towards some transition

* Corresponding author. Mobile: +91 9245165958; fax: +91 4562 281338.
E-mail address: drn_raman@yahoo.co.in (N. Raman).

0022-2860/$ - see front matter © 2010 Elsevier B.V. All rights reserved.
doi:10.1016/j.molstruc.2010.10.038

elements, which may help more in understanding the mode of chelation of Schiff base and mixed ligands towards metals. For this purpose the mixed-ligand complexes of Cu(II) and VO(IV) ions with Schiff bases as main ligands and polypyridyl ligands as co-ligands, are studied both in solution and solid state. Binding to DNA is usually accompanied by marked absorbance changes in the UV–Vis, due to excitation of charge-transfer transitions [16]. DNA-interaction studies of titled complexes were investigated by electronic spectrum, cyclic voltammetry and gel electrophoresis so as to explore the mode and effect. The biological activity of the parent Schiff base and its metal complexes were also investigated. Information obtained from our study would be helpful in understanding the mechanism of interactions of the complexes with nucleic acid and might also be useful in the development of potential probes of DNA structure and conformation, and new therapeutic reagents for some uncommon diseases.

2. Experimental section

2.1. Reagents and standard solutions

CT DNA, gel loading buffer, Tris base, 4-amino-2-3-dimethyl-1-phenyl-3-pyrazolin-5-one, 1,10-phenanthroline and 2,2′-bipyridine were purchased from Sigma–Aldrich. Ethidium bromide (EB), calf thymus DNA (CT DNA) and pBR322 plasmid DNA were also purchased from Sigma. All other chemicals used were of analytical reagent grade and were used without any further purification.

All the experiments involved in the interaction of the ligand and its metal complexes with CT DNA were carried out in doubly distilled water buffer containing 5 mM Tris [Tris(hydroxymethyl)–aminomethane] and 50 mM NaCl and adjusted to pH 7.1 with hydrochloric acid. Solution of CT DNA in Tris–HCl buffer gave ratio of UV absorbance of about 1.8–1.9:1 at 260 and 280 nm, indicating that the CT DNA was sufficiently free of protein [17]. The CT DNA concentration per nucleotide was determined spectrophotometrically by employing an extinction coefficient of 6600 M^{-1} cm^{-1} at 260 nm [18].

2.2. Equipments

UV–Vis, spectra were recorded on a Shimadzu Model 1601 UV–Visible Spectrophotometer. IR spectra of the ligand and its metal complexes were recorded on a Perkin-Elmer FTIR-1605 spectrophotometer using KBr discs. The intensity of the reported IR signals were defined as w = weak, m = medium and s = strong. ^{1}H NMR spectra were measured on a Varian XL-300 MHz spectrometer with tetramethylsilane (TMS) as the internal standard at room temperature. The complexes were analyzed for their metal contents, following standard procedures [19] after decomposition with a mixture of conc. HNO_3 and HCl, followed by conc. H_2SO_4. Microanalyses (C, H, N) were carried out on a Perkin–Elmer 240 elemental analyzer. Mass spectrometry experiments were performed on a JEOL-AccuTOF JMS-T100LC mass spectrometer equipped with a custom-made electrospray interface (ESI). The X-band EPR spectra of the complexes were recorded at RT (300 K) and LNT (77 K) using TCNE as the g-marker. Room temperature magnetic susceptibility measurements were carried out on a modified Gouy-type magnetic balance, Hertz SG8-5HJ. X-ray diffraction experiments were carried out on XPERT-PRO diffractometer system. Copper Kα_1 line, with wavelength of 1.5406 Å generated with a setting of 30 mA and 40 kV with the electrodes, was used for diffraction. The slit width setting was 91 mm. The diffracting angle (2θ) was scanned from 10.0251 to 79.9251 continuously with a rate of 2° per minute. The whole process took place at a temperature of 25°C. The thermal analyses measurements (TGA and DTG) were carried out on a Setaram Labsys TG-16 thermobalance under nitrogen atmosphere. The molar conductivity of the complexes in DMF solution (10^{-3} M) was measured using the conductometer model 601/602.

Voltammetric experiments were performed on a CHI 620C electrochemical analyzer in freshly distilled DMF solutions. 0.1 M tetrabutylammonium perchlorate (TBAP) was used as the supporting electrolyte. The three-electrode cell comprised a reference Ag/AgCl, auxiliary Pt and the working Glassy Carbon electrodes. All the solutions examined by electrochemical techniques were purged with nitrogen for 10 min prior to each set of experiments. All measurements were carried out at room temperature (25 °C).

2.3. Synthesis of the Schiff base ligands (dbdppo/hnbdppo)

The Schiff bases under investigation were prepared by mixing an ethanol solution (25 mL) of 4-amino-2-3-dimethyl-1-phenyl-3-pyrazolin-5-one (2.032 g, 0.01 mol) with 3,4-dimethoxybenzaldehyde (1.66 g, 0.01 mol) or 3-hydroxy-4-nitrobenzaldehyde (1.67 g, 0.01 mol) in the same volume of ethanol and was refluxed for 3 h in water bath and the obtained appropriate precipitate was collected and recrystallized from ethanol.

4-(3′,4′-dimethoxybenzaldehydene)2-3-dimethyl-1-phenyl-3-pyrazolin-5-one is a light yellow colored crystal with an yield of 89%, Anal. Calcd. (%) $C_{20}H_{21}N_3O_3$; M.W: 351.40, C(68.36%), H(6.02%), N(11.95%), found (%) C(68.25%), H(5.92%), N(11.48%); ^{1}H NMR (DMSO-d_6) δ: 3.28(s, 3H, P_Z—N—CH_3), 2.26(s, 3H, P_Z—C—CH_3), 3.92(s, 3H, O—CH_3), 6.97–7.40(m, 3H, Ph), 6.90–7.37(m, 5H, Ph), 8.01(s, 1H, N=CH); IR(KBr) ν(cm^{-1}): 1634(s) (HC=N), 1308(s) (O—CH_3), 1281(s) (Pz—C—CH_3), 1181(s) (Pz—N—CH_3), 1714(s) (Pz—C=O), 1471(s) (Ph—C=C), 1545(m) (Ph—C—C), 3048(s) (Ph—C—H); UV–Vis (DMF) [nm(frequency, cm^{-1})(transition)(geometry)]; 387(25,839) (ILCT), 352(28,409) (ILCT), 264(37,878) (ILCT).

4-(3′-hydroxy-4′-nitrobenzaldehydene)2-3-dimethyl-1-phenyl-3-pyrazolin-5-one is a yellow colored powder with an yield of 90%, Anal. Calcd. (%) $C_{18}H_{16}N_4O_4$; M.W: 352.35, C(61.35%), H(4.57%), N(15.90%), found(%) C(68.25%), H(4.43%), N(15.48%); ^{1}H NMR (DMSO-d_6) δ: 3.11(s, 3H, P_Z—N—CH_3), 2.58(s, 3H, P_Z—C—CH_3), 10.28(s, 1H, OH), 6.77–7.15(m, 3H, Ph), 6.90–7.37(m, 5H, Ph), 8.00(s, 1H, N=CH); IR (KBr) ν(cm^{-1}): 1614(s) (HC=N), 1608(w) (C—NO_2), 3442(b) (OH), 1293(s)(Pz—C—CH_3), 1145(s) (Pz—N—CH_3), 1710(s) (Pz—C=O), 1423(s) (Ph—C=C), 1530(m) (Ph—C—C), 3075(s) (Ph—C—H); UV–Vis, (DMF) [nm(frequency, cm^{-1})(transition)(geometry)]; 399(25,062) (ILCT), 364(27,472) (ILCT), 270(37,037) (ILCT), 248(40,322) (ILCT).

2.4. Synthesis of new Cu(II) and VO(IV) complexes

All the new Cu(II) and VO(IV) complexes were prepared by the following general procedure as sketched in Scheme 1. To an ethanolic solution of the appropriate Schiff base (0.001 mol), metal salts (0.001 mol) in ethanol (15 mL) were added and kept stirring for 30 min. To the above stirring solution, about 0.001 mol of 2,2′-bipyridine (bpy)/1,10-phenanthroline (phen) in the appropriate ratio was added (Scheme 1) and refluxed for 2–3 h. The resultant product was washed and recrystallized with ethanol.

[Cu(dbdppo)(bpy)$_2$](Cl)$_2$ (1): Green powder, yield 67%, M.F: $[CuC_{40}H_{37}N_7O_3]Cl_2$, M.Wt: 798.23, Anal. Calcd. (%) C(60.21%), H(4.73%), N(12.32%), Cu(7.97%) found (%) C(60.15%), H(4.65%), N(12.27%), Cu(7.94%); IR(KBr) ν(cm^{-1}): 1566(strong, s) (HC=N), 1316(s) (O—CH_3), 1248(s) (Pz—C—CH_3), 1158(s) (Pz—N—CH_3), 1644(s) (Pz—C=O), 1473(s) (Ph—C=C), 1536(m) (Ph—C—C), 3052(s) (Ph—C—H), 479(m) (M—N), 578(m) (M—O); UV–Vis, (DMF) [nm(frequency, cm^{-1})(transition)(geometry)]; 965(10,362) ($^2B_{1g} \rightarrow {}^2B_{2g}$) [Octahetral($O_h$)], 770(12,987) ($^2B_{1g} \rightarrow {}^2A_{1g}$)($O_h$), 386(25,906) (ILCT), 327(30,581) (ILCT), 243(41,152) (ILCT).

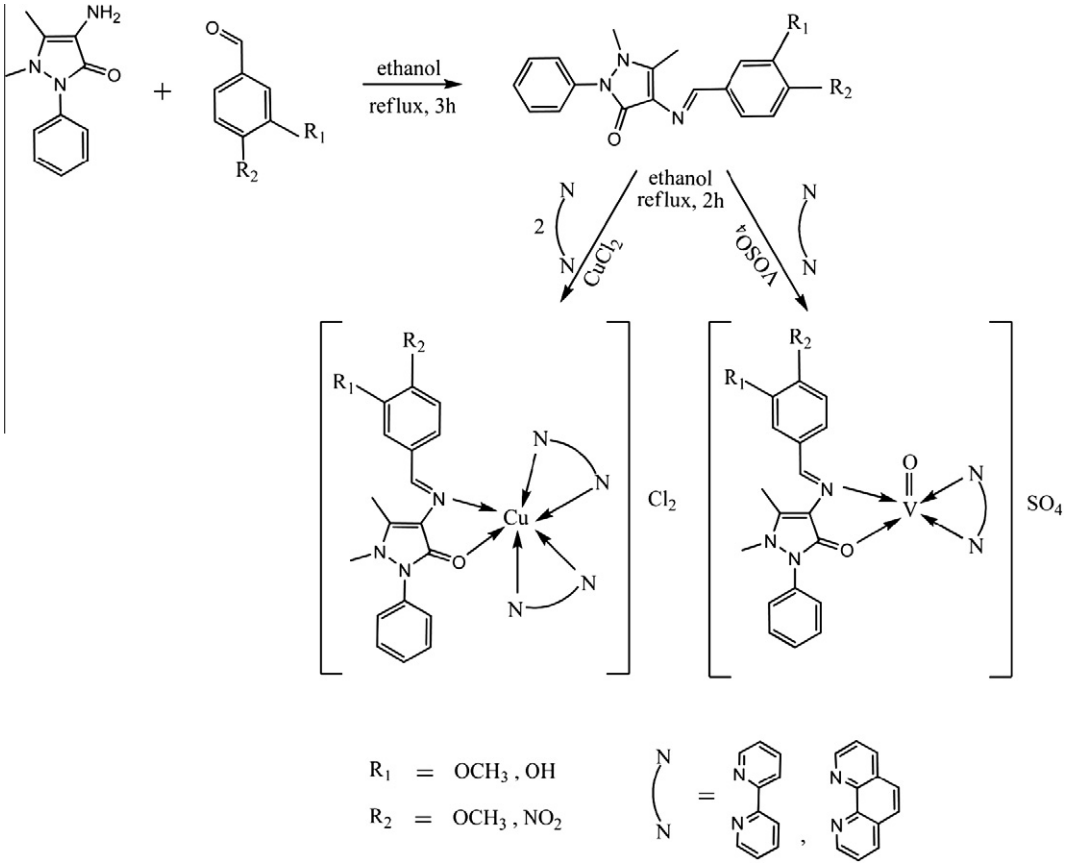

Scheme 1. Synthetic route for metal complexes.

[Cu(dbdppo)(phen)$_2$](Cl)$_2$ (2): Green powder, yield 72%, M.F: [$CuC_{44}H_{37}N_7O_3$]Cl_2, M.Wt: 846.27, Anal. Calcd. (%) C(62.51%), H(4.43%), N(11.59%), Cu(7.53%) found (%) C(62.43%), H(4.38%), N(11.57%), Cu(7.47%); IR(KBr) ν(cm^{-1}): 1548(s) (HC=N), 1354(s) (O—CH_3), 1292(s) (Pz—C—CH_3), 1137(s) (Pz—N—CH_3), 1652(s) (Pz—C=O), 1452(s) (Ph—C=C), 1537(m) (Ph—C—C), 3109(s) (Ph—C—H),482(m) (M—N), 585(m) (M—O); UV–Vis, (DMF) [nm(frequency, cm^{-1})(transition)(geometry)]; 975(10,256) ($^2B_{1g} \rightarrow {}^2B_{2g}$) ($O_h$), 720(13,888)($^2B_{1g} \rightarrow {}^2A_{1g}$)($O_h$), 386(25,906) (ILCT), 266(37,593) (ILCT).

[Cu(hnbdppo)(bpy)$_2$](Cl)$_2$ (3): Green powder, yield 68%, M.F: [$CuC_{38}H_{32}N_8O_4$]Cl_2, M.Wt: 799.17, Anal. Calcd. (%) C(57.21%), H(4.12%), N(14.15%), Cu(7.97%) found (%) C(57.10%), H(4.01%), N(14.03%), Cu(7.93%); IR (KBr) ν(cm^{-1}): 1579(s) (HC=N), 1601(w) (C-NO_2), 3439(b) (OH), 1296(s)(Pz—C—CH_3), 1159(s) (Pz—N—CH_3), 1659(s) (Pz—C=O), 1444(s) (Ph—C=C), 1530(m) (Ph—C—C), 3052(s) (Ph—C—H), 504(m) (M—N), 596(m) (M—O); UV–Vis, (DMF) [nm(frequency, cm^{-1}) (transition)(geometry)]; 1022(9784) ($^2B_{1g} \rightarrow {}^2B_{2g}$) ($O_h$), 721(13,869)($^2B_{1g} \rightarrow {}^2A_{1g}$)($O_h$), 443(22,573) (ILCT), 215(46,511) (ILCT).

[Cu(hnbdppo)(phen)$_2$](Cl)$_2$ (4): Green powder, yield 75%, M.F: [$CuC_{42}H_{32}N_8O_4$]Cl_2, M.Wt: 847.21, Anal. Calcd. (%) C(59.61%), H(3.84%), N(13.27%), Cu(7.53%) found (%) C(59.53%), H(3.76%), N(13.18%), Cu(7.48%); IR (KBr) ν(cm^{-1}): 1549(s) (HC=N), 1602(w) (C—NO_2), 3576(w) (OH), 1315(s)(Pz—C—CH_3), 1117(s) (Pz—N—CH_3), 1651(s) (Pz-C=O), 1470(s) (Ph—C=C), 1528(m) (Ph—C—C), 3082(s) (Ph—C—H), 468(m) (M—N), 575(m) (M—O); UV–Vis, (DMF) [nm(frequency, cm^{-1}) (transition) (geometry)]; 980(10,204) ($^2B_{1g} \rightarrow {}^2B_{2g}$) ($O_h$), 702(14,245)($^2B_{1g} \rightarrow {}^2A_{1g}$)($O_h$), 445(22,471) (ILCT), 302(33,112) (ILCT), 241(41,493) (ILCT).

[VO(dbdppo)(bpy)](SO$_4$) (5); Green powder, yield 68%, M.F: [$VOC_{30}H_{29}N_5O_3$]SO_4 M.Wt: 654.58, Anal. Calcd. (%) C(55.07%), H(4.51%), N(10.72%), VO(7.81%) found (%) C(54.99%), H(4.43%), N(10.69%), VO(7.78%); IR(KBr) ν(cm^{-1}): 1598 (s) (HC=N), 1332(s) (O—CH_3), 1292(s) (Pz—C—CH_3), 1181(s) (Pz—N—CH_3), 1659(s) (Pz—C=O), 960(s) (V=O), 1471(s) (Ph—C=C), 1545(m) (Ph—C—C), 3052(s) (Ph—C—H), 465(m) (M—N), 582(m) (M—O); UV–Vis, (DMF) [nm(frequency, cm^{-1})(transition)(geometry)]; 979(10,214) ($^2B_2 \rightarrow {}^2E$) (Square-Pyramidal (SP), 877(11,402) ($^2B_2 \rightarrow {}^2B_1$)(SP), 386(25,906) (ILCT).

[VO(dbdppo)(phen)](SO$_4$) (6): Green powder, yield 72%, M.F: [$VOC_{32}H_{29}N_5O_3$]SO_4 M.Wt: 678.61, Anal. Calcd. (%) C(56.63%), H(4.35%), N(10.34%), VO(7.56%) found (%) C(56.58%), H(4.27%), N(10.31%), VO(7.50%); IR(KBr) ν(cm^{-1}): 1589(s) (HC=N), 1302(s) (O—CH_3), 1258(s) (Pz—C—CH_3), 1137(s) (Pz—N—CH_3), 1649(s) (Pz-C=O), 984(s) (V=O), 1483(s) (Ph—C=C), 1532(m) (Ph—C—C), 3071(s) (Ph—C—H), 507(s) (M—N), 587(m) (M—O); UV–Vis, (DMF) [nm(frequency, cm^{-1}) (transition) (geometry)]; 1022 (9784) ($^2B_2 \rightarrow {}^2E$), (SP) 640(15,625) ($^2B_2 \rightarrow {}^2B_1$)(SP), 377(26,525) (ILCT), 302(33,112) (ILCT).

[VO(hnbdppo)(bpy)](SO$_4$) (7): Green powder, yield 63%, M.F: [$VOC_{28}H_{24}N_6O_4$]SO_4 M.Wt: 655.53, Anal. Calcd. (%) C(51.27%), H(3.72%), N(12.87%), VO(7.81%) found (%) C(51.25%), H(3.66%), N(12.81%), VO(7.77%); IR(KBr) ν(cm^{-1}): 1587(s) (HC=N), 1611(w) (C—NO_2), 3433(b) (OH), 1292(s)(Pz—C—CH_3), 1163(s) (Pz—N—CH_3), 1651(s) (Pz—C=O), 960(s) (V=O), 1441(s) (Ph—C=C), 1523(m) (Ph—C—C), 3077(s) (Ph—C—H), 503(m) (M—N), 552(m) (M—O); UV–Vis, (DMF) [nm(frequency, cm^{-1})(transition)(geometry)]; 977(10,235) ($^2B_2 \rightarrow {}^2E$) (SP), 853(11,723) ($^2B_2 \rightarrow {}^2B_1$)(SP), 395(25, 316) (ILCT), 284(35,211) (ILCT).

[VO(hnbdppo)(phen)](SO_4) (8): Green powder, yield 65%, M.F: $[VOC_{30}H_{24}N_6O_4]SO_4$ M.Wt: 679.55, Anal. Calcd. (%) C(53.01%), H(3.62%), N(12.43%), VO(7.52%) found (%) C(52.97%), H(3.53%), N(12.36%), VO(7.49%); IR (KBr) ν(cm^{-1}): 1578(m) (HC═N), 1626(w) (C—NO_2), 3451(b) (OH), 1304(s) (Pz—C—CH_3), 1162(s) (Pz—N—CH_3), 1654(s) (Pz—C═O), 975(s) (V═O), 1438(s) (Ph—C═C), 1524(m) (Ph—C—C), 3084(s) (Ph—C—H), 479(m) (M—N), 567(m) (M—O); UV–Vis, (DMF) [nm(frequency, cm^{-1})(transition)(geometry)]; 984(10,162) ($^2B_2 \rightarrow {}^2E$) (SP), 858(11,655) ($^2B_2 \rightarrow {}^2B_1$) (SP), 372(26,881) (ILCT), 267(37,453) (ILCT).

2.5. Pharmacology

In vitro antibacterial, antifungal assay and chemical nuclease activity of the synthesized compounds are described in the Supplementary file.

3. Results and discussion

The complexes were prepared by direct reaction of Schiff base ligand(s) and bpy/phen with the appropriate molar ratios of Cu(II) chloride and VO(IV) sulphate in ethanol. The yields were good to moderate. The desired Cu(II) and VO(IV) complexes were separated from the solution by suction filtration, purified by washing several times with ethanol. The complexes were air-stable for extended periods and soluble in DMSO and DMF; slightly soluble in ethanol and methanol; insoluble in benzene and water. The molar conductivities of the complexes were around 218.3–227.5 Ω^{-1} cm^2 mol^{-1} in DMF solution, showing that all complexes were electrolytes. FTIR spectral data supported that the copper ion in all complexes has N_5O coordination sphere and oxovanadyl ion in all complexes has N_3O_2 coordination sphere, bound by oxygen in pyrazole ring, imine and pyridine type nitrogen atoms. The spectroscopic studies and analytical data supported our proposed structure (Scheme 1).

3.1. IR spectra and coordination mode

IR spectra have proven to be the most suitable technique to give enough information to elucidate the nature of bonding of the ligand to the metal ion. The IR spectra of the ligands and two representative complexes are shown in Fig. S1 (Supplementary file). The IR spectra of the free Schiff base ligands **dbdppo** and **hnbdppo** show moderate intensity absorptions at 1634 and 1614 cm^{-1} respectively attributable to the imine ν (C═N) [20,21] and 1714 and 1710 cm^{-1} bands are observed for free ν(C═O) of **dbdppo** and **hnbdppo** ligands respectively and no bands are observed for free primary amine indicating that complete condensation has occurred between 4-aminoantipyrine and 3,4-disubstituted benzaldehyde supporting the formation of Schiff base. The coordination of the ligands with different metals through the nitrogen atom is expected to reduce the electron density in the azomethine link and lower the ν(C═N) absorption frequency. This shift in absorption of the ν(C═N) frequency in case of the complexes suggests the coordination through the nitrogen of (>C═N) group [22]. A strong to medium intensity band in ligands due to the presence of ν(C═O) groups, which is shifted towards lower frequency after complexation, which proves the coordination with metal [21]. This displacement can be attributed to the electronic donation of the base to metal (N → M), which increases the electron density on the metal d-orbitals, and consequently the $p_\pi \rightarrow d_\pi$ donation from the oxygen atom to metal is expected to be reduced [23]. This behavior indicates the fact that the carbonyl oxygen atom of the antipyrine residue is coordinated. The IR values, ν(C–H) 862 cm^{-1} and 736 cm^{-1} observed for phenanthroline are red shifted to 854 cm^{-1} and 725 cm^{-1}. These shifts can be explained by the fact that each of the two nitrogen atoms of phenanthroline ligands donate a pair of electrons to the central metal forming a coordinate covalent bond [24,25].

Metal–ligand bond is further confirmed by the appearance of a medium intensity band in the range 465–507 and 552–596 cm^{-1} in the spectra of the complexes assigned to stretching frequencies of (M–N) bond [26,27] and metal–oxygen bond formation [28] respectively and this can be explained by the donation of electrons from nitrogen or oxygen to the empty d-orbitals of the metal atom. In addition to other bands, the vanadyl complexes show a strong band at 984–960 cm^{-1}, attributed to the stretching vibration of the terminal V═O bond [29,30,21].

3.2. Electronic spectra and magnetic measurement

Visible spectral data along with magnetic susceptibility measurements gave adequate support in establishing the geometry of the metal complexes. These data along with the assignments are presented in experimental. The electronic spectra of ligands and complexes were recorded in DMF solution in the scan range 200–1100 nm. In the electronic spectra of the ligand and its mononuclear metal complexes, the wide range bands were observed due to either the $\pi \rightarrow \pi^*$ and $n \rightarrow \pi^*$ of C═N chromophore or charge-transfer transition arising from π electron interactions between the metal and ligand, which involves either a metal-to-ligand or ligand-to-metal electron transfer [31,32]. The absorption bands between 352 and 399 nm in free ligands change a bit in intensity for metal complexes. The absorption shift and intensity change in the spectra of the metal complexes most likely originate from the metalation which increases the conjugation and delocalization of the whole electronic system and results in the energy change of $\pi \rightarrow \pi^*$ and $n \rightarrow \pi^*$ transition of the conjugated chromophore [33]. These results clearly indicate that the ligand coordinates to Cu(II) and VO(IV) ions, which are in accordance with the results of the other spectral data.

Furthermore, the electronic spectra of six coordinate copper(II) complexes have either D_{4h} or C_{4v} symmetry, and the e_g and t_{2g} level of the ^2D free ion term will split into B_{1g}, A_{1g}, B_{2g} and E_g levels, respectively under the influence of the distortion, can be such as to cause the two transitions, $^2B_{1g} \rightarrow {}^2B_{2g}$ and $^2B_{1g} \rightarrow {}^2A_{1g}$ which are represented in experimental part. This supports the distorted octahedral copper(II) complex which is usual in the d^9 case [34,35]. The magnetic moment of 1.78–1.97 BM falls within the range normally observed for octahedral Cu(II) complexes [36].

The electronic spectra of the vanadyl complexes show two absorption bands and their transitions corresponding to five-coordinate square-pyramidal geometry [37] which are represented in experimental part. This is also supported by the magnetic moment value in the range of 1.68–1.76 BM observed for the five-coordinate VO(IV) complexes. Suggested structures of the complexes are given in Scheme 1.

3.3. Mass spectra

The ESI mass spectrum gives additional structural information about the stereochemistry of the studied compounds. The mass spectrum of the studied compound is characterized by moderate to high relative intensity molecular ion peaks. It is obvious that the molecular ion peaks are in good agreement with their suggested empirical formula as indicated from elemental analyses. The ESI mass spectrum of **3** shows a molecular ion (M^+) peak at m/z = 728, which suggests the monomeric nature of the complex and confirms the proposed formula. The ESI mass spectrum of **hnbdppo** Schiff base shows a molecular ion peak m/z at 352 which is equivalent to its molecular weight and also exhibits two additional peaks m/z at 353 and 354, which are corresponding to

(M+1) and (M+2) peaks respectively. The spectrum of **hnbdppo** also shows a series of peaks corresponding to various fragments which are shown in Scheme 2. Their intensity gives an idea of the stability of the fragments and also about the geometrical configurations.

3.4. EPR spectra

The EPR spectra of copper(II) complexes provide information about hyperfine and super hyperfine structures. It is very important to understand the metal ion environment in the complexes, *i.e*., the geometry, nature of the donating atoms from the ligands and degree of covalency of the copper(II)–ligands bonds. The ESR spectra of the Cu(II) complexes were recorded in DMSO at liquid nitrogen temperature (LNT) and at room temperature (RT). EPR spectra of the copper(II) complexes are given in Figs. S2 and S3 (Supplementary file). *g*-Tensor values of copper(II) complexes can be used to derive the ground state. In an elongated octahedron, the 3d unpaired electrons for copper(II) ion lies in d_{x2-y2} orbital ($^2B_1$ as ground state). In addition, exchange coupling interaction between two Cu(II) ions is explained by Hathaway expression $G = (g_{||} - 2)/(g_{\perp} - 2)$. When the value $G < 4.0$, a considerable exchange coupling is present in solid complex. It has been reported (Table 1) that $g_{||}$ value of copper(II) complex can be used as a measure of the covalent character of the metal–ligand bond. If the value is more than 2.3, the metal–ligand bond is essentially ionic and the value less than 2.3 is indicative of covalent character [38]. The covalency parameter (α^2) indicates considerable covalent

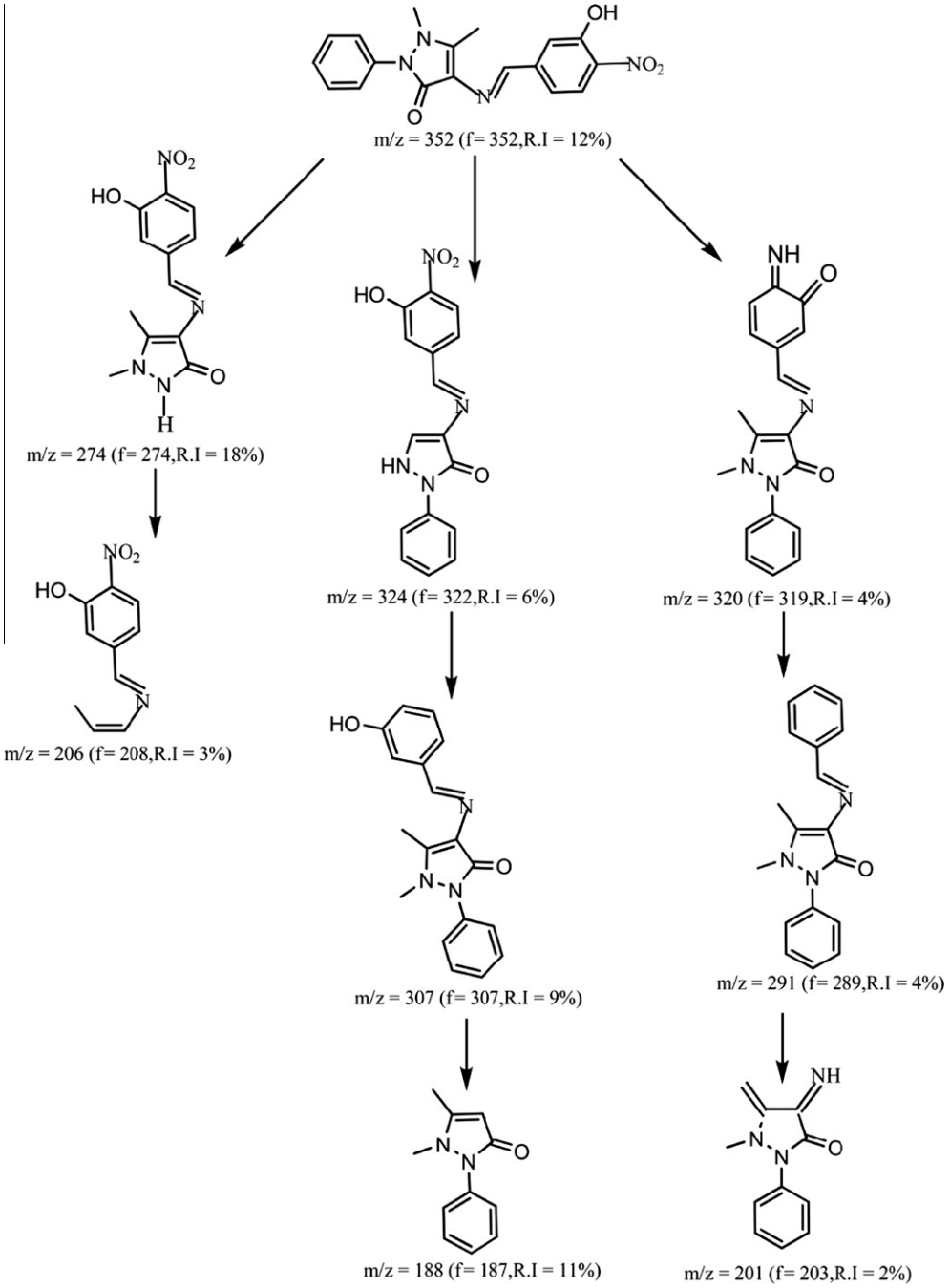

Scheme 2. Mass fragment pattern of **hnbdppo** ligand.

Table 1
The spin Hamiltonian parameters of Cu(II) complexes in DMSO at 300 K and 77 K.

Complex	g-Tensor			Hyperfine constant $\times 10^{-4}$ cm^{-1}		
	$g_{\|}$	$g_{\perp}$	g_{iso}	$A_{\|}$	$A_{\perp}$	A_{iso}
1	2.1726	2.0695	2.1038	240	30	100
2	2.1766	2.0732	2.1076	250	40	110
3	2.1686	2.0659	2.1001	250	20	96.6
4	2.1807	2.0768	2.1114	240	30	100

character for the metal–ligand bond [39]. Also the trend $g_{||} > g_{\perp} > g_e$ (2.0027) observed for these complexes indicates that the unpaired electron is most likely in the d_{x2-y2} orbital of the Cu(II) ion in complexes [40]. The ESR spectra only show signals that may be accounted for the presence of free radicals that can be resulted from the cleavage of any double bond and distribution of the charge on the two neighbor atoms. The peaks are broad and have the appearance of ill-resolved triplets. The breadth and triplet appearance can be attributed to hyperfine splitting by the nitrogen atom (I = 1) of the ligand. The triplet appearance is adduced as an evidence for nitrogen coordination. The spin Hamiltonian parameters suggest that the copper ion is strongly distorted from planar geometry which is in good agreement with electronic absorption spectral data.

The EPR parameters $g_{||}$, $g_{\perp}$, g_{av}, $A_{||}$ and $A_{\perp}$ and the energies of the d–d transitions were used to evaluate the bonding parameters (Table 2) α^2, β^2 and γ^2 which may be regarded as measurement of covalency of the in-plane σ-bonding, in-plane π-bonding and out of plane π-bonding respectively. The value of α^2 and β^2 were estimated from the following expression [41].

$$\alpha^2 = -(A||/0.036) + (g|| - 2.0023) + (3/7)(g_{\perp} - 2.0023) + 0.04 \quad (1)$$

$$\beta^2 = (g|| - 2.0023)\mathrm{E}/ - 8\lambda\alpha^2 \quad (2)$$

According to Hathaway [42], $K_{||} \approx K_{\perp} \approx 0.77$ for pure in-plane σ-bonding and $K_{||} < K_{\perp}$ for in-plane π-bonding, while for out of plane π-bonding $K_{||} > K_{\perp}$. In all the Cu(II) complexes, it is observed that $K_{||} < K_{\perp}$ which indicates the presence of significant of in-plane π-bonding than from out of plane π-bonding in metal–ligand π-bonding. K is dimensionless quantity, which is a measure of the contribution of s electrons to the hyperfine interaction and is generally found to have a value of 0.30. The K values obtained for all the complexes are in agreement with those estimated by Assour [43] and Abragam and Pryce [44].

Hence, the EPR study of the copper(II) complexes has provided supportive evidence to the conclusion obtained on the basis of electronic spectrum and magnetic moment values. Thus, the results confirmed that, the Cu(II) complexes possess distorted octahedral geometry.

3.5. Powder X-ray diffractogram

To obtain further evidence about the structure of the metal complexes X-ray diffraction was performed. The powder X-ray diffractogram study of the complexes **1** and **3** (Fig. 1) has been carried out to understand the lattice dynamics of the complexes. The observed interplanar spacing values ('*d*' in *A*°), 2 angles and the Miller indices (*h k l*) values are listed in Table 3. The X-ray powder diffractograms of **1** and **3** complexes were recorded using Cu Kα as the source in the 2θ range 10.02–79.92°. The X-ray powder diffraction patterns throws light only on the fact that each solid represents a definite compound of a definite structure which is not contaminated with starting materials. The X-ray data revealed that the copper complexes had crystallized in the face-centered cubic system [45]. The azomethine of **1** and **3** exhibited two main reflections at 2 = 24.30° and 24.36°, respectively (*d* spacing 3.66 and 3.65 Å, respectively).

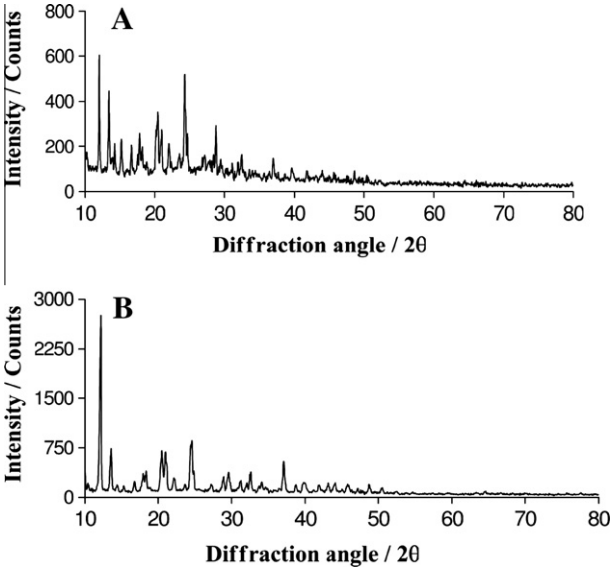

Fig. 1. Powder X-ray diffraction pattern of (A) **1** and (B) **3** complexes.

Finally, the above data indicate that the coordination occurs through the nitrogen of the pby/phen ring, azo-methine nitrogen atom and oxygen present in pyrazole ring to give the structures as shown in Scheme 1.

3.6. Thermal properties of the ligand and its metal complexes

The thermal properties of the ligand and its metal complexes investigated by thermal gravimetric analysis (TGA) and differential thermogravimetry (DTG) are presented in the Supplementary file.

3.7. Pharmacological results

The results of antibacterial, antifungal and chemical nuclease activity of the compounds are given and discussed in the Supplementary file.

3.8. Electrochemical study of complexes

Analysis of cyclic voltammograms with scan rates varying from 0.06 to 0.18 V s^{-1} shows that the process is diffusion controlled

Table 2
The bonding parameters of Cu(II) complexes in DMSO solution.

Complex	α^2	β^2	γ^2	$K_{\|}$	$K_{\perp}$	$K \times 10^{-4}$ (cm^{-1})	G
1	0.9051	0.4066	0.6394	0.3331	0.5617	138.8	2.5434
2	0.9385	0.3057	0.4957	0.2692	0.5912	150.2	2.4666
3	0.9273	0.2849	0.4342	0.2450	0.5292	134.0	2.6250
4	0.9163	0.3265	0.5438	0.2742	0.6374	141.7	2.4021

Table 3
X-ray powder diffraction data of the **1** and **3** mixed ligand Schiff base complexes.

1			**3**		
2θ	Lattice spacing (d) (Å)	$h\ k\ l$	2θ	Lattice spacing (d) (Å)	$h\ k\ l$
12.008	7.3644	2 0 0	12.124	7.2942	2 0 0
17.836	4.9688	2 2 0	17.913	6.5381	2 2 0
20.956	4.2355	3 1 1	20.480	4.3329	3 1 1
27.078	3.2903	3 3 1	21.020	4.2228	2 2 2
28.746	3.1030	4 2 0	24.548	3.6234	4 0 0
32.408	2.7603	5 1 1	27.214	3.2741	3 3 1
41.774	2.1605	5 3 3	32.526	2.7505	3 3 3
45.674	1.9847	7 1 1	39.819	2.2620	0 2 6
48.614	1.8713	6 4 2	45.805	1.9793	6 4 0

and coupled to relatively fast chemical complications. Electrochemical properties of the complexes were studied on a Pt disc electrode in DMF containing 0.05 M n-Bu_4NClO_4 as the supporting electrolyte. As a typical case, in the case of complex **2**, the one-electron reduction peak, which is attributed to the Cu(II)/Cu(I) couple, occurs at $E_{pc} = -0.785$ V, with an associated reoxidation peak in the reverse scan at $E_{pa} = -0.262$ V as shown in Fig. S4 (Supplementary file). The most interesting observation in the region appears to be a well defined redox couple for which the anodic peak potential corresponds to the oxidation [46] of Cu(II)/Cu(III) and the cathodic counter part is due to the reduction of Cu(III).

The cathodic peak current of the complexes increased and the peak potentials were shifted towards more negative direction with an increase in scan rate. The difference in the cathodic and anodic peaks suggests that the process involves transfer of one electron and therefore corresponds to a Cu(II)/Cu(I) and Cu(III)/Cu(II) couples. The difference between forward and backward peak potential scan provides a rough evaluation of the degree of the reversibility. The peak-to-peak potential separation (ΔE_p) of the electrode couples increased with increase in the scan rate confirming the occurrence of a slow chemical reaction and a limited mass transfer following the electrode process [47].

For Pt electrodes, when plotting cathodic peak current (I_{pc}) against the sweep rates, linear plots were observed as shown in Fig. S4 (inset). This clearly demonstrates that the electron transfer process within the film exhibits the characteristic features of a surface bound species [48]. Similarly the cyclic voltammetric behaviors of vanadyl complexes have also been studied and the data are presented in Table 4.

3.9. Binding characteristics of complex with DNA

The transition metal complexes are known to bind with DNA *via* both covalent and/or noncovalent interactions [49]. In covalent binding, the labile ligand of the complexes is replaced by a nitrogen base of DNA such as guanine N7. On the other hand, the noncovalent DNA interactions include intercalative, electrostatic and groove (surface) binding of metal complexes along outside the DNA helix, along major or minor groove. It has been reported that DNA can provide three distinctive binding sites for quinolone metal complexes; namely, groove binding, electrostatic binding to phosphate group and intercalation [50]. This behavior is of great importance with regard to the relevant biological role of quinolone antibiotics in the body [51].

3.9.1. Electronic absorption titration with CT DNA

The binding of metal complexes to CT DNA have been studied through the changes in absorbance and shift in wavelength. As hypochromism and hyperchromism are both the spectral features of DNA concerning its double helix structure, hypochromism means the DNA binding mode of a complex *via* electrostatic effect or intercalation whereas hyperchromism means the breakage of the secondary structure of DNA on binding of the complex. The absorption spectra of metal complexes in the absence and presence of CT DNA are shown in Fig. 2A and B. With increasing concentration of CT DNA, the absorption band of the complex is affected, resulting in the obvious tendency of hypochromism and blue shift. It is clear from the spectra that, in the case of bipyridine complexes where the bpy rings are not coplanar, only a moderate hypochromism is observed compared to phen complexes. The intrinsic binding constants K_b of the two complexes with CT DNA were obtained by monitoring the changes in the intraligand band with increasing concentration of DNA using the following function equation;

$$[DNA]/(\varepsilon_a - \varepsilon_f) = [DNA]/(\varepsilon_b - \varepsilon_f) + 1/[K_b(\varepsilon_b - \varepsilon_f)]$$

where [DNA] is the concentration of DNA in base pairs, the apparent absorption coefficient ε_a, ε_f and ε_b correspond to A_{obs}/[complex], the extinction coefficient for the free metal complexes and the extinc-

Table 4
Electrochemical behavior of Cu(II) and VO(IV) complexes in the presence of CT DNA.

Complex	Redox couple	$I_{pc}(A) \times 10^{-5}$		E_{pc} (V)		$E_{1/2}$ (V)		ΔE_p (V)		K_{oxd}/K_{red}
		Free	Bound	Free	Bound	Free	Bound	Free	Bound	
1	Cu(III)/Cu(II)	0.89	0.85	−0.079	−0.057	0.135	0.322	0.428	0.436	2.35
	Cu(II)/Cu(I)	1.56	1.10	−0.602	−0.585	0.294	−0.356	0.616	0.458	1.94
2	Cu(III)/Cu(II)	0.772	0.718	−0.111	−0.103	0.130	0.125	0.482	0.457	1.36
	Cu(II)/Cu(I)	1.51	0.99	−0.785	−0.759	−0.523	−0.520	0.523	0.477	2.75
3	Cu(III)/Cu(II)	0.54	0.47	−0.066	−0.042	0.120	0.115	0.372	0.315	2.54
	Cu(II)/Cu(I)	1.02	0.84	−0.533	−0.524	−0.342	−0.349	0.381	0.349	1.42
4	Cu(III)/Cu(II)	0.42	0.38	−0.028	−0.055	0.010	0.022	0.770	0.154	0.35
	Cu(II)/Cu(I)	1.79	1.45	−0.789	−0.772	−0.492	−0.499	0.593	0.546	1.93
5	VO(IV)/VO(III)	5.49	2.69	−0.637	−0.604	−0.569	−0.616	0.136	−0.024	3.61
6	VO(IV)/VO(III)	1.32	0.62	−0.851	−0.807	−0.729	−0.755	0.244	0.103	5.55
7	VO(IV)/VO(III)	1.84	1.51	−0.811	−0.764	−0.790	−0.756	0.042	0.016	6.24
8	VO(IV)/VO(III)	1.83	1.19	−0.827	−0.811	−0.787	−0.777	0.080	0.068	1.86

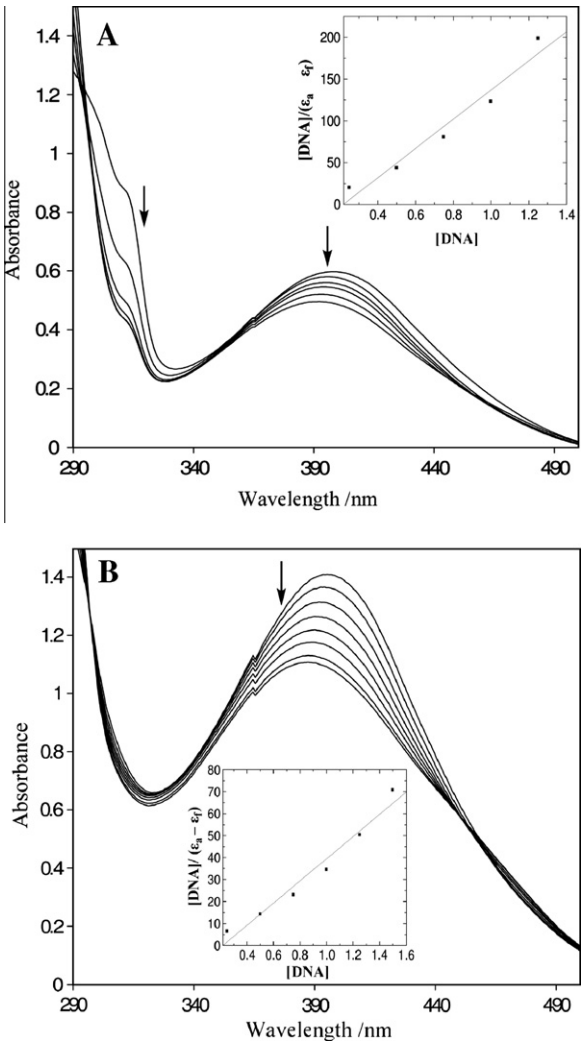

Fig. 2. Absorption spectra of complex (A) **3** and (B) **7** in the presence of DNA in Tris–HCl buffer upon addition of CT DNA. [complex] = 25 μM. Arrow shows the absorbance changing upon the increase of DNA concentration.

tion coefficient for the free metal complexes in the fully bound form, respectively. In plots of [DNA]/($\varepsilon_a - \varepsilon_f$) *versus* [DNA], K_b is given by the ratio of slope to the intercept.

To compare quantitatively the affinity of the complexes toward DNA, the intrinsic binding constants K_b were $2.59 \times 10^6\ M^{-1}$ with hypochromicity 68.9% for **4**, $4.61 \times 10^5\ M^{-1}$ with hypochromicity 16.75% for **3**, $4.27 \times 10^5\ M^{-1}$ with hypochromicity 65.5% for **2**, $3.49 \times 10^5\ M^{-1}$ with hypochromicity 47.91% for **1**, $3.08 \times 10^6\ M^{-1}$ with hypochromicity 19.8% for **8**, $4.59 \times 10^5\ M^{-1}$ with hypochromicity 18.2% for **7**, $4.19 \times 10^5\ M^{-1}$ with hypochromicity 23.0% for **6**, $3.84 \times 10^5\ M^{-1}$ with hypochromicity 6.6% for **5** respectively which are comparable with other Cu(II) and VO(IV) phen/bpy mixed-ligand complexes [52–54]. This may be due to the introduction of two substituents reducing the planarity and the different shape of the intercalating ligand. For complexes **3** and **4**, the **hnbdppo** ligand possessed appropriate planarity and possibly supported by the formation of an intramolecular hydrogen bond between the ortho phenolic group and the oxygen atom of nitro moiety and overlap with the base pairs of DNA. While for complexes **1** and **2**, the two substituents of bulky methoxy group reduced the planarity and steric hindrance may arise when the complex containing the intercalative ligand **dbdppo** interacts with DNA. On the other hand, the higher binding affinity of complex **4** to DNA than that of complex **3** may be due to the greater planar area of phen, thus resulting in higher hydrophobicity of phen than that of bpy. These data indicate that the extent of hypochromism commonly parallels the intercalative strength of the ligand and, moreover, a higher planar area, an extended π system, hydrophobicity, and aromaticity lead to deep penetration and hence more stacking within the base pairs of DNA.

3.9.2. Electrochemical titration with CT DNA

CV has proved to be a very sensitive analytical technique to determine changes in redox behavior of metallic species in the presence of biologically important molecules [55,56].The electrochemical investigations of metal–DNA interactions can provide a useful complement to spectroscopic methods, *e.g.*, for nonabsorbing species, and yield information about interactions with both the reduced and oxidized form of the metal [57]. The quasi-reversible redox couple for each complex in DMF solution that has been studied upon addition of CT DNA and the shifts of the E_{pc}, $E_{1/2}$ and ΔE_p is given in Table 4.

Cyclic voltammetric technique has been applied to study the interaction of the present redox active copper(II) complexes with DNA with a view to further explore the DNA binding modes assessed from the spectral and viscometric studies. The cyclic voltammogram at Pt disk electrode for copper(II) complexes display two one electron quasi-reversible peaks, Cu(II)/Cu(I) and Cu(II)/Cu(III) redox couples (Fig. 3). It is known that the redox potential of Cu(II)/Cu(I) process is shifted towards more negative potential as the electron-donating ability of the substituents on the ligand framework becomes higher [58]. The co-ordination chemistry of high oxidation state metal complexes is very important because of their biological significance as redox enzyme models. Only a small number of ligands have an ability to stabilize the high oxidation state of copper. **dbdppo** ligand, which possesses the strong donating ability of methoxy groups which can stabilize the high oxidation state of metal complexes.

The Cu(II)/Cu(I) and Cu(II)/Cu(III) redox processes are influenced by the coordination number, stereochemistry and the hard/soft character of the ligands, donor atoms However due to inherent difficulties in relating coordination number and stereochemistry of the species present in solution, redox processes are generally described in terms of the nature of the ligands present [59]. Patterson and Holm [60] have shown that softer ligands tend to produce more positive *E* values, while hard acids give rise to negative E values. The observed *E* values for the **1–4** complexes indicate considerable "hard acid" character, as reported earlier [61]. This is likely to be due to azo-methine nitrogen donor and nitrogen atoms of the heterocyclic bases involved in coordination.

It can be observed (Table 4) that complexes **1–4** exhibit the same electrochemical behavior upon addition of CT DNA. Upon addition of CT DNA, both the cathodic and anodic peak currents decrease very remarkably. The drop of the voltammetric currents in the presence of CT DNA can be attributed to diffusion of the metal complex bound to the large, slowly diffusing DNA molecule [62]. The more pronounced decrease of the peak currents upon addition of CT DNA, the stronger the binding affinity of the complex to DNA. Partial intercalation mode, as deduced above, can account for this [63]. The shift in $E_{1/2}$ for Cu(II) complexes on binding to DNA suggests that both Cu(II) and Cu(I) forms bind to DNA but to different extents.

The cyclic voltammogram (CV) studies for the oxovanadium (IV) complexes **5–8** were realized in DMF solutions. The electrochemical data are summarized in Table 4. For all the complexes one quasi-reversible wave were observed. Based on these observations, it is reasonable to suggest that the reduction process may involve the stepwise redox processes depicted below:

$$VO(IV) \rightleftharpoons VO(III) \quad (3)$$

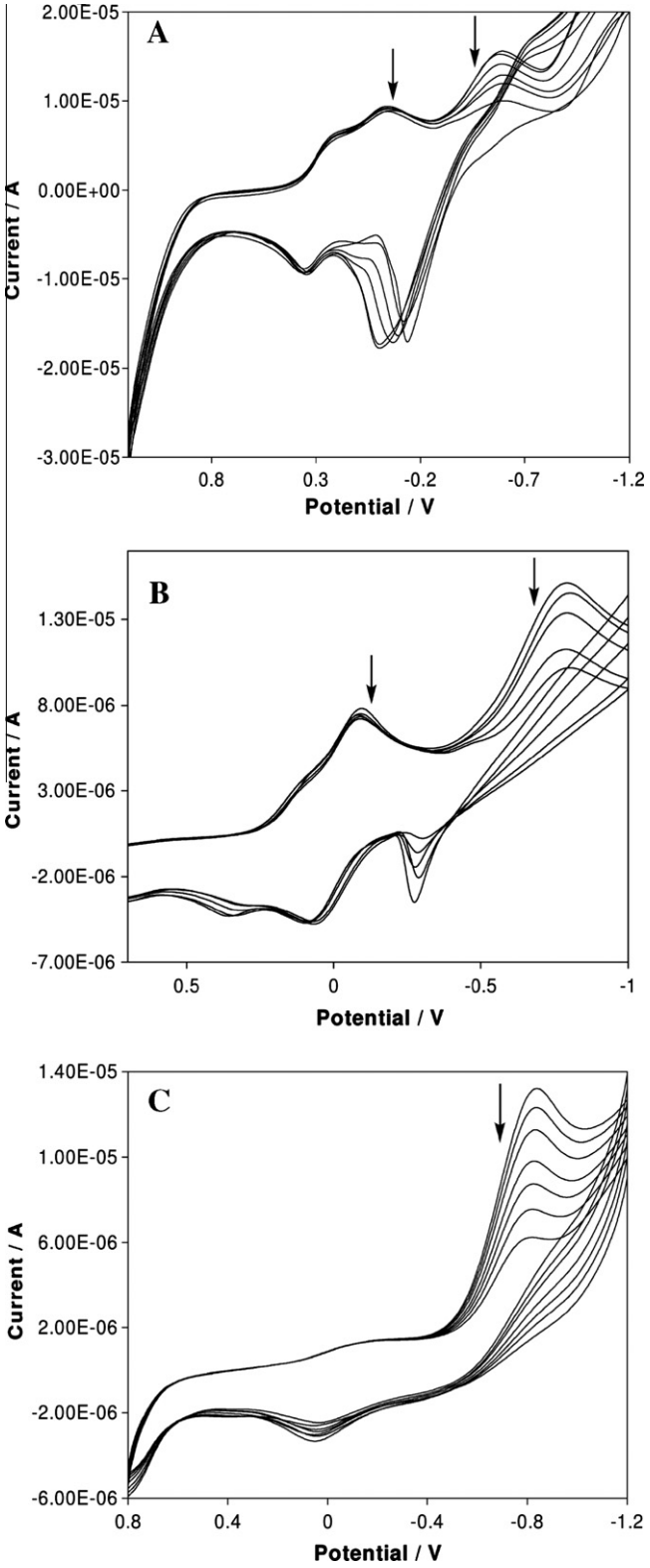

Fig. 3. Cyclic voltammogram in DMF:buffer [mixture 50 mM Tris–HCl/NaCl buffer (pH, 7.2)] (1:2) solution of (A) **1** (scan rate = 0.1 V s^{-1}), (B) **2** (scan rate = 0.08 V s^{-1}) and (C) **6** (scan rate = 0.12 V s^{-1}) with incremental addition of CT DNA. 0.05 M n-Bu_4NClO_4 as supporting electrolyte and the arrow mark indicates the current changes upon increasing DNA concentrations.

The redox potentials of the complexes are in the range ($E_{1/2}$) −0.569 to −0.790 V, and are assigned to the vanadyl ion present in the azomethine moiety. The more negative potentials of the quasi-reversible peaks are assigned to reduction of the vanadyl(IV) ion. As shown in Fig. 3C, for the CV curve of complex **6**, the VO(IV)/VO(V) redox processes are irreversible, in accord with the observed behavior for other similar vanadium(IV) complexes [64,65]. It was also observed that the ligands moiety has a significant effect on $E_{1/2}$ for **5** and **6**; electron-withdrawing groups stabilize the VO(IV) in the complexes while the electron-donating groups favor oxidation to VO(V). This is possibly because the electron-withdrawing anion makes the complex more positively charged and it favors the reduction of metal ion. Similarly the electron-donating groups make the complexes less positively charged. Electropotential of VO(IV)/VO(V) couple is showing sensitivity to the nature of atoms in ligands moiety.

From the cyclic voltammetric studies it can be stated that the complexes containing more aromatic rings get reduced at higher negative potentials than the complexes containing less aromatic rings. The higher reduction potential can be attributed due to the greater planarity and electronic properties that are associated with aromatic rings [66].

CV study shows that the complexes **5–8** exhibit the same electrochemical behavior upon addition of CT DNA. For increasing amounts of CT DNA, the cathodic potential Epc shows a positive shift (ΔE_{pc} = +33 mV for **5**, ΔE_{pc} = +44 mV for **6** (Fig. 3C), ΔE_{pc} = +47 mV for **7** and ΔE_{pc} = +16 mV for **8**) while the anodic potentials Epa shift to negative values (ΔE_{pa} = −127 mV for **5**, ΔE_{pa} = −97 mV for **6**, ΔE_{pa} = −21 mV for **7** and ΔE_{pa} = −4 mV for **8**). These shifts of the potentials show that complexes **5–8** can bind to DNA by both intercalation and electrostatic interaction [67,68].

On comparing the cyclic voltammograms, we observe that the variation in oxidation and reduction potential may be due to distortion in geometry that arises due to different metals in coordination and also the difference in $E_{1/2}$, values which further support to the involvement of number of co-ligands in coordination and nature of substituents on the ligands moiety.

Differential Pulse Voltammograms (DPV) of **2** and **6** (10^{-3} M) in the absence and presence of varying addition of DNA are shown in Fig. S5 (Supplementary file). It was observed that a significant reduction in cathodic peak current of **2** and **6** decreased on the addition of DNA is due to slow diffusion of an equilibrium mixture of the free and DNA-bound complexes to the electrode surface and its potential shifted after reacting with DNA, which was consistent with the results of the cyclic voltammetry.

The decrease in the peak current of complex **2** and **6** resulted from the addition of DNA into **2** and **6** solution in CV and DPV can be employed to determine the binding constant (K). The binding behavior of **2** and **6** to DNA was measured by keeping the concentration of the **2** and **6** constant while varying the concentration of the DNA by using the response of the one electron CV and DPV step of the Cu(II)/Cu(I) and Cu(III)/Cu(II) for **2** and VO(IV)/VO(III) for **6** during the addition of DNA solution. K_+/K_{2+} value for the **2** suggesting that the preferential stabilization of Cu(II) form over Cu(III) and Cu(I) forms on binding to DNA. DPV of the complexes as a function of added DNA also indicates a large decrease in current intensity with a small shift in formal potential due to the partial intercalative interaction of complexes.

3.9.3. Viscosity measurements

A useful technique to prove intercalation is viscosity measurements, which are sensitive to length change of DNA and regarded as the least ambiguous and the most critical tests of binding mode in solution in the absence of crystallographic structural data or NMR spectra [69]. Under appropriate conditions, intercalation of drugs like ethidium bromide (EB) causes a significant increase in viscosity of DNA solution due to the increase in separation of base pairs of intercalation sites and hence results in an increase in overall DNA contour length. On the other hand, drug molecules binding

exclusively in the DNA grooves cause less pronounced or no changes in DNA solution viscosity [70]. A classical intercalation model demands that the DNA helix must lengthen as base pairs are separated to accommodate the binding ligand, leading to the increase of DNA viscosity. In contrast, a partial and/or non-classical intercalation of ligand bend (or kink) the DNA helix, reduce its length and, concomitantly, its viscosity [70].

The effects of complexes **1–8**, together with $[Ru(bpy)_3]^{2+}$ and EB on the viscosity of rod-like DNA are shown in Fig. 4. EB increases the relative specific viscosity for the lengthening of the DNA double helix through the intercalation mode, while complex $[Ru(bpy)_3]^{2+}$, which has been known to bind with DNA in electrostatic mode, exerts essentially no effect on DNA viscosity. Viscosity of CT DNA (200 μM) has been measured in the presence of varying amount of complexes **1–8** (20–140 μM), the relative viscosity of DNA increased steadily, which is similar to the behavior of EB. In addition, the relative viscosities of DNA increase with the order of **hnbdppo** > **dbdppo** complexes. This order suggests the extent of the unwinding and lengthening of DNA helix by compounds and the affinities of compounds binding to DNA, which may be due to the key roles of substituent effects and the larger coplanar structure of the complexes than those of ligands. Intercalation has been traditionally associated with molecules containing bpy/phen ring structures which can bind to DNA through intercalation. The results suggest that the above complexes intercalate the base pairs of DNA, which is consistent with the result observed in absorption titration curves.

4. Conclusions

Binary Schiff base and pby/phen complexes having essential oxygen, azomethine and nitrogens were prepared and structurally characterized. The correlation of the experimental data allows assigning an octahedral geometry for Cu(II) and square-pyramidal geometry for VO(IV) ions. The redox active Cu(II) and VO(IV) complexes exhibit significant photo-induced DNA cleavage activity as evidenced from their ability to convert SC pBR322 DNA to its linear form upon excitation with UV-light irradiation at 365 nm. The DNA cleavage reaction was found to follow a photo-redox mechanistic pathway that generates reactive hydroxyl radical species. The better binding properties of the complexes should be attributed to the good coplanarity of the ligand after coordination with metal ions.

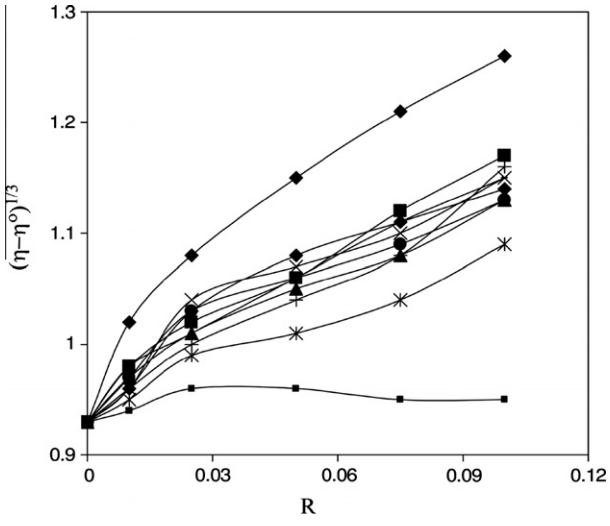

Fig. 4. Effect of increasing amounts of EB (♦), $[Ru(bpy)_3]^{2+}$(■) and in presence of increasing concentrations of complexes of **1** (●), **2** (♦), **3** (+), **4** (■), **5** (∗), **6** (▲), **7** (_), **8** (×) on the relative viscosity of CT-DNA at 30 °C. [DNA] = 1.5 mM, R = [complex]/[DNA] or [EB]/[DNA].

Meanwhile, nature of the substituents present in the Schiff base ligands and central metal ions also affected the intercalative ability. These results indicate that DNA might also serve as the primary target of these compounds; in addition, they should have many potential practical applications, just like the promising therapeutic drug candidates. In the cyclic voltammograms of the complexes recorded in DMF, in all cases, quasi-reversible waves attributed to redox couples, characteristic for each metal complex, have been recorded at potentials expected for the central metal ions. The substituents at different positions on intercalative ligand can cause some interesting differences in the properties of the resulting complexes. On the basis of chelation theory, metal complexes have more biological activity than the free ligands.

Acknowledgment

The authors express their sincere thanks to the College Managing Board, Principal and Head of the Department of Chemistry, VHNSN College for providing necessary research facilities and financial support. Instrumental facilities provided by Sophisticated Analytical Instrument Facility (SAIF) IIT Bombay and CDRI Lucknow are gratefully acknowledged.

Appendix A. Supplementary material

Supplementary data associated with this article can be found, in the online version, at doi:10.1016/j.molstruc.2010.10.038.

References

[1] I.D. Capel, M. Jenner, M.H. Pinnock, D.C. Williams, Biochem. Pharmacol. 27 (1978) 1413.
[2] S. Bondock, R. Rabie, H.A. Etman, A.A. Fadda, Eur. J. Med. Chem. 43 (2008) 2122.
[3] S. Cunha, S.M. Oliveira, M. Rodrigues Jr., R.M. Bastos, J. Ferrari, O.C. de, L. Kato, H.B. Napolitano, I. Vencato, C. Lariucci, J. Mol. Struct. 752 (2005) 32.
[4] M.A. Madiha, A. Rania, H. Moataz, S. Samira, B. Sanaa, Eur. J. Pharmacol. 569 (2007) 222.
[5] G. Turan-Zitouni, M. Sivaci, F.S. Kilic, K. Erol, Eur. J. Med. Chem. 36 (2001) 685.
[6] T. Bansal, M. Singh, G. Mishra, S. Talegaonkar, R.K. Khar, M. Jaggi, R. Mukherjee, J. Chromatogr. B 859 (2007) 261.
[7] J.S. Casas, M.S. García-Tasende, A. Sánchez, J. Sordo, A. Touceda, Coord. Chem. Rev. 251 (2007) 1561.
[8] N.V. Bashkatova, E.I. Korotkova, Y.A. Karbainov, A.Y. Yagovkin, A.A. Bakibaev, J. Pharmaceut. Biomed. 37 (2005) 1143.
[9] S.S.A.E. Rehim, M.A.M. Ibrahim, K.F. Khalid, Mater. Chem. Phys. 70 (2001) 268.
[10] M.S. Collado, V.E. Mantovani, H.C. Goicoechea, A.C. Olivieri, Talanta 52 (2000) 909.
[11] K.Y. Lau, A. Mayr, K.K. Cheung, Inorg. Chim. Acta 285 (1999) 223.
[12] Z. Travnıcek, M. Malon, Z. Sindelar, K. Dolezal, J. Rolcık, V. Krystof, M. Strnad, J. Marek, J. Inorg. Biochem. 84 (2001) 23.
[13] X.J. Yang, F. Drepper, B. Wu, W.H. Sun, W. Haehnel, C. Janiak, Dalton Trans. (2005) 256.
[14] L.F. Tan, F. Wang, H. Chao, Y.F. Zhou, C. Weng, J. Inorg. Biochem. 101 (2007) 700.
[15] Y.B. Zeng, N. Yang, W.S. Liu, N. Tang, J. Inorg. Biochem. 97 (2003) 258.
[16] M.E. Cucciolito, A.D. Renzi, F. Giordano, F. Ruffo, Organometallics 14 (1995) 5410.
[17] Y.Z. Cai, Q. Luo, M. Sun, H. Corke, Life Sci. 74 (2004) 2157.
[18] K.E. Heim, A.R. Tagliaferro, D.J. Bobilya, J. Nutr. Biochem. 13 (2002) 572.
[19] Vogel, A Text Book of Quantitative Inorganic Analysis, third ed., ELBS, Longman, London, 1969.
[20] C.R.K. Rao, P.S. Zacharias, Polyhedron 16 (1977) 1201.
[21] T. Rosu, M. Negoiu, S. Pasculescu, E. Pahontu, D. Poirier, A. Gulea, Eur. J. Med. Chem. 45 (2010) 774.
[22] E. Tas, A. Kilic, M. Durgun, L. Küpecik, I. Yilmaz, S. Arslan, Spectrochim. Acta Part A 75 (2010) 811.
[23] A.L. Doadrio, J. Sotelo, A. Fernandez-Ruano, Quim. Nova 25 (2002) 525.
[24] L. Jin, P. Yang, Polyhedron 16 (1997) 3395.
[25] R. Senthil Kumar, S. Arunachalam, Polyhedron 26 (2007) 3255.
[26] S. Chandra, L.K. Gupta, Spectrochim. Acta Part A 61 (2005) 269.
[27] S.A. Patil, V.H. Naik, A.D. Kulkarni, P.S. Badami, Spectrochim. Acta Part A 75 (2010) 347.
[28] S. Chandra, R. Kumar, Trans. Met. Chem. 29 (2004) 269.
[29] P.K. Sasmal, A.K. Patra, A.R. Chakravarty, J. Inorg. Biochem. 102 (2008) 1463.
[30] E.K. Efthimiadou, A. Karaliota, G. Psomas, J. Inorg. Biochem. 104 (2010) 455.
[31] E. Tas, M. Aslanoglu, A. Kilic, Z. Kara, J. Coord. Chem. 59 (8) (2006) 861.

[32] M. Odabasoglu, F. Arslan, H. Olmez, O. Buyukgungor, Dyes Pigm. 75 (3) (2007) 507.
[33] Z. Chen, Y. Wu, D. Gu, F. Gan, Acta A 68 (3) (2007) 918.
[34] M.V. Angelusiu, S.F. Barbuceanu, C. Draghici, G.L. Almajan, Eur. J. Med. Chem. 45 (2010) 2055.
[35] V.P. Singh, A. Katiyar, Pestic. Biochem. Physiol. 92 (2008) 8.
[36] F.A. Cotton, G. Wilkinson, C.A. Murillo, M. Bochmann, Advanced Inorganic Chemistry, sixth ed., Wiley, New York, 1999.
[37] Z.H. Chohan, S.H. Sumrra, M.H. Youssoufi, T.B. Hadda, Eur. J. Med. Chem. 45 (2010) 2739.
[38] P. Kamalakannan, D. Venkappayya, Russ. J. Coord. Chem. 28 (2002) 423.
[39] S.N. Shetti, A.S.R. Murty, G.L. Tembe, Indian J. Chem. 32A (1993) 318.
[40] K.B. Gudasi, S.A. Patil, R.S. Vadavi, R.V. Shenoy, Trans. Met. Chem. 31 (2006) 586.
[41] D. Kivelson, R. Neiman, J. Chem. Soc., Dalton Trans. 35 (1961) 149.
[42] B.J. Hathaway, Structure and Bonding, vol. 14, Springer-Verlag, Heidelberg, 1973. p. 60.
[43] M. Assour, J. Chem. Phys. 43 (1965) 2477.
[44] A. Abragam, M.H.L. Pryce, Roy. Soc. Lond. A 206 (1951) 164.
[45] M. Bicer, I. Sisman, Powder Technol. 198 (2010) 279.
[46] S. Djebbar-Sid, O. Benali-Baitich, J.P. Deloume, Polyhedron 16 (1997) 2175.
[47] N.C. Paramanik, S. Bhatacharya, Polyhedron 16 (1997) 1755.
[48] C. Stinner, M.D. Wightman, S.O. Kelley, M.G. Hill, J.K. Barton, Inorg. Chem. 40 (2001) 5245.
[49] Q.L. Zhang, J.G. Liu, J. Liu, G.Q. Xue, H. Li, J.Z. Liu, H. Zhou, L.H. Qu, L.N. Ji, J. Inorg. Biochem. 85 (2001) 291.
[50] B.M. Zeglis, V.C. Pierre, J.K. Barton, Chem. Commun. 44 (2007) 4565.
[51] G.S. Son, J.A. Yeo, M.S. Kim, S.K. Kim, A. Holmen, B. Akerman, B. Norden, J. Amer. Chem. Soc. 120 (1998) 6451.
[52] F. Arjmand, M. Aziz, Eur. J. Med. Chem. 44 (2009) 834.
[53] N. Raman, R. Jeyamurugan, A. Sakthivel, L. Mitu, Spectrochim. Acta Part A 75 (2010) 88.
[54] P.K. Sasmal, A.K. Patra, A.R. Chakravarty, J. Inorg. Biochem. 102 (2008) 1463.
[55] S. Srinivasan, J. Annaraj, P.R. Athappan, J. Inorg. Biochem. 99 (2005) 876.
[56] A.M. Leone, J.D. Tibodeau, S.H. Bull, S.W. Feldberg, H.H. Thorp, R.W. Murray, J. Am. Chem. Soc. 125 (2003) 6784.
[57] M.T. Carter, A.J. Bard, J. Am. Chem. Soc. 109 (1987) 7528.
[58] P.M. Bush, Inorg. Chem. 40 (2001) 1871.
[59] B.J. Hathaway, in: G. Wilkinson, R.D. Gillard, J.A. McCleverty (Eds.), Comprehensive Coordination Chemistry, vol. 4, Pergamon Press, Oxford, 1987.
[60] G.S. Patterson, R.H. Holm, J. Bioinorg Chem. 4 (1975) 1257.
[61] P. Bindu, M.R.P. Kurup, Met. Chem. 22 (1997) 578.
[62] J. Sun, D.K.Y. Solaiman, J. Inorg. Biochem. 38 (1990) 169.
[63] J. Liu, T.X. Zhang, T.B. Lu, L.H. Qu, H. Hui, Q.L. Zhang, L.N. Ji, J. Inorg. Biochem. 91 (2002) 269.
[64] P.I.S. Maia, V.M. Deflon, E.J. Souza, E. Garcia, G.F. de Sousa, A.A. Batista, A.T. Figueiredo, E. Niquet, Transit. Met. Chem. 30 (2005) 404.
[65] V.M. Deflon, D.M. Oliveira, G.F. de Sousa, A.A. Batista, L.R. Dinelli, E. Castellano, Z. Anorg. Allg. Chem. 628 (2002) 1140.
[66] J. Manonmani, R. Thirumurugan, M. Kandaswamy, V. Narayanan, M.N. Ponnuswamy, G. Shanmugam, H.K. Fun, Polyhedron 20 (2001) 3039.
[67] K. Jiao, Q.X. Wang, W. Sun, F.F. Jian, J. Inorg. Biochem. 99 (2005) 1369.
[68] G. Psomas, J. Inorg. Biochem. 102 (2008) 1798.
[69] S. Satyanarayana, J.C. Dabroniak, J.B. Chaires, Biochemistry 31 (1992) 9319.
[70] S. Satyanarayana, J.C. Dabrowiak, J.B. Chaires, Biochemistry 32 (1993) 2573–2584.